Towards production of novel catalyst powders from supported size-selected clusters by multilayer deposition and dicing

Jian, Nan; Bauer, Karl; Palmer, Richard E

DOI:
10.1088/1361-6528/aa795b

Document Version
Publisher's PDF, also known as Version of record

Citation for published version (Harvard):
Jian, N, Bauer, K & Palmer, RE 2017, 'Towards production of novel catalyst powders from supported size-selected clusters by multilayer deposition and dicing', *Nanotechnology*, vol. 28, no. 32, pp. 325601. https://doi.org/10.1088/1361-6528/aa795b

Towards production of novel catalyst powders from supported size-selected clusters by multilayer deposition and dicing

OPEN ACCESS
IOP Publishing
Nanotechnology

Nanotechnology **28** (2017) 325601 (7pp)
https://doi.org/10.1088/1361-6528/aa795b

Towards production of novel catalyst powders from supported size-selected clusters by multilayer deposition and dicing

Nan Jian[1], **Karl Bauer**[1] **and Richard E Palmer**[2]

[1] Nanoscale Physics, Chemistry and Engineering Research Laboratory, School of Physics and Astronomy, University of Birmingham, Birmingham, B15 2TT, United Kingdom
[2] College of Engineering, Swansea University, Swansea, SA1 8EN, United Kingdom

E-mail: Nanjianbai@163.com

Received 16 February 2017, revised 28 May 2017
Accepted for publication 14 June 2017
Published 18 July 2017

Abstract

A multilayer deposition method has been developed with the potential to capture and process atomic clusters generated by a high flux cluster beam source. In this deposition mode a series of sandwich structures each consisting of three layers—a carbon support layer, cluster layer and polymer release layer—is sequentially deposited to form a stack of isolated cluster layers, as confirmed by through-focal aberration-corrected HAADF STEM analysis. The stack can then be diced into small pieces by a mechanical saw. The diced pieces are immersed in solvent to dissolve the polymer release layer and form small platelets of supported clusters.

Keywords: cluster, multilayer deposition, electron microscopy, dicing

(Some figures may appear in colour only in the online journal)

1. Introduction

Understanding and tailoring the novel properties of nanoclusters (nanoparticles) has been a longstanding cornerstone of nanoscience research [1–4]. Nanoclusters display unique and highly size-dependent physical and chemical properties, providing potential for use in, e.g., electronics, optics, biology and catalysis applications [1–9]. There are three major cluster production routes: physical vapour (e.g. cluster beam) deposition, chemical synthesis, and biological formation [5, 10–18]. Compared with many examples of chemical and biological synthesis routes, cluster beam deposition has several potential advantages: the possibility of precise size control by means of a mass filter; a tunable interaction with the deposition support (by control of the cluster beam impact energy); and convenience in producing multi-elemental clusters [18].

However, despite such advantages, cluster beam technology has not been industrialized on a large scale. The greatest issue limiting the commercial exploitation of cluster beam technology is the low cluster deposition flux, which to date has made this route uncompetitive compared with the chemical synthesis methods [11, 18]. To address this issue a new cluster beam technique, the matrix assembly cluster source (MACS), has been developed in our laboratory, which shows significant potential for scaling up the cluster beam flux to the milligram and eventually gram scale: or equivalently, to increase conventional cluster beam currents of the order of nanoamps or below to the microamp and milliamp regimes [19–21]. A significant challenge arising is then how to accommodate and process this large abundance of clusters. The conventional cluster sources allow deposition onto planar substrates, a few square centimetres in area [11, 18]. However, the MACS has the potential to cover with clusters an area of square metres (and in future beyond) in a matter of minutes. Therefore, a new deposition scheme, which is capable of accommodating and exploiting the high cluster flux is required. In particular, one wishes to collect the clusters as individual entities without aggregation on the support.

Here we present the proof of principle of a novel multilayer cluster deposition scheme that we believe is potentially scalable to cope with the kind of cluster beam flux available from high flux cluster sources such as the MACS. The key element of this scheme is the sequential deposition of a stack of three-layer sandwiches each comprising: (a) a thin support film, (b) a sub-monolayer of clusters, and (c) a soluble release layer. The stack of sandwich structures is then diced into small pieces and immersed in a solvent to dissolve the soluble release layers and create small platelets covered with clusters. Polyvinyl pyrrolidone (PVP) is a water soluble polymer of low toxicity which is also soluble in many organic solvent. It is also a standard stabilizer in colloidal synthesis of, e.g., catalytic nanoparticles [22–28]. For our proof of principle demonstration, PVP layers (either spray-deposited using a pulse valve or evaporated) were used as release layers, the support film was a carbon film produced using a direct-current evaporator or an e-beam evaporator, and the cluster layer comprised size-selected Au_{923} clusters generated by a magnetron sputtering inert gas condensation cluster source [11] (thus in the demonstration a conventional cluster source only is employed). The characterization of the multilayer structure was performed using through-focal measurements with the aberration-corrected high angle annular dark field scanning transmission electron microscope (HAADF STEM).

2. Experimental section

The carbon support layers were produced with either a direct current evaporator or a SPECS EBE-1 e-beam evaporator, which were added to the deposition chamber of the magnetron cluster source [11]. The thickness of the carbon layer was controlled by an integrated flux monitor. The carbon support film was simultaneously deposited on both a $1 \times 1\,cm^2$ silicon substrate and a 400-mesh TEM grid (for the STEM characterization of the multilayer structure). Size-selected Au_{923} clusters were deposited onto the carbon support layer from a gas condensation magnetron sputtering cluster source equipped with a lateral time-of-flight mass selector [11, 29, 30]. The chosen nominal mass resolution of the cluster source was $M/\Delta M \approx 20$. The deposition energy of the clusters was set to 0.54 eV per atom by controlling the bias applied to the substrates for deposition. The PVP (average molecular weight 10 000 Daltons; Sigma-Aldrich) release layer was deposited on top of the cluster layer by either pulse valve spray deposition or thermal evaporation. The spray deposition was performed using a First Sensor series-9 high performance pulse valve. The thermal evaporation was performed using a home-built thermal evaporator. The dicing of the samples was performed using a diamond saw (DAD321 Automatic Dicer). Then the diced samples were immersed in isopropanol to dissolve the PVP release layers to produce the small supported cluster platelets. The multilayer stacks, before and after dicing, and the final released material were analysed with a JEOL JEM 2100F HAADF STEM, equipped with a spherical aberration corrector (CEOS GmbH). The acceleration voltage employed was 200 kV. The convergence angle of the electron probe was 19 mrad. The HAADF detector utilized a 62 mrad inner angle and 164 mrad outer angle. To minimize the effect of the sample's roughness level on the through-focal HAADF STEM analysis, the through focal analysis was performed in a region smaller than 31 nm × 31 nm.

3. Results and discussion

A schematic of the multilayer deposition process is shown in figure 1. The method results in the production of a stack of carbon–cluster–PVP sandwiches. To test the method, an 8-sandwich sample was produced (using identical deposition conditions for each sandwich trilayer) on a TEM grid for aberration-corrected STEM analysis. This measurement technique has been successfully employed to obtain 3D information on dopants, buried defects and even single atoms using through-focal analysis [31–34]. An illustrative schematic of the through-focal method and the corresponding experimental HAADF STEM images are shown in figure 2. In a sample comprising two carbon–cluster–PVP sandwiches, when the electron beam is focused on the upper Au cluster, an image of a clear upper Au cluster and blurry lower Au cluster is obtained. Then, the electron beam is focused on the lower cluster. Assuming the focal planes are located at the centre of the clearly imaged clusters, the focal difference between these two focal planes can be considered as the thickness of one carbon–cluster–PVP repeat unit.

In the analysis of our 8-sandwich sample, six distinct layers of Au clusters were observed by the through-focal HAADF STEM, as shown in figure 3. The focal range was from −28–13 nm. The focal differences between the neighbouring layers were 9, 9, 9, 8 and 6 nm, moving from the low defocus to high defocus values. These values indicate the corresponding thicknesses of the sandwiches. This result shows the reliable deposition of the different layers: the thickness of each sandwich is quite uniform, especially in the case of the first four layers. We note that the influence of the carbon and PVP deposition on the clusters seems to be minimal. We can see that the sizes and shapes of most clusters are preserved from aggregation, even for clusters that close to each other in the same layer (e.g. the two clusters circled in figure 3(d)); see also below.

It was not possible to identify clusters from all eight discrete cluster layers in a single STEM image. At most, it was only possible to identify clusters from six discrete layers in one image. The reason for this may be the relatively small lateral region we used for the through-focal analysis. The sample cannot be aligned exactly normal to the electron beam, so to minimize the effect of this the analysis region is set to be no larger than 31 nm × 31 nm. In this small region, due to the modest lateral cluster density, it is hard to find clusters from all eight layers. Evidence of the missing layers can be found in other series of the through-focal HAADF STEM images. For example, in a second series, only four layers of Au clusters were identified, but the focal difference between the highest and lowest cluster layers is 47 nm, which

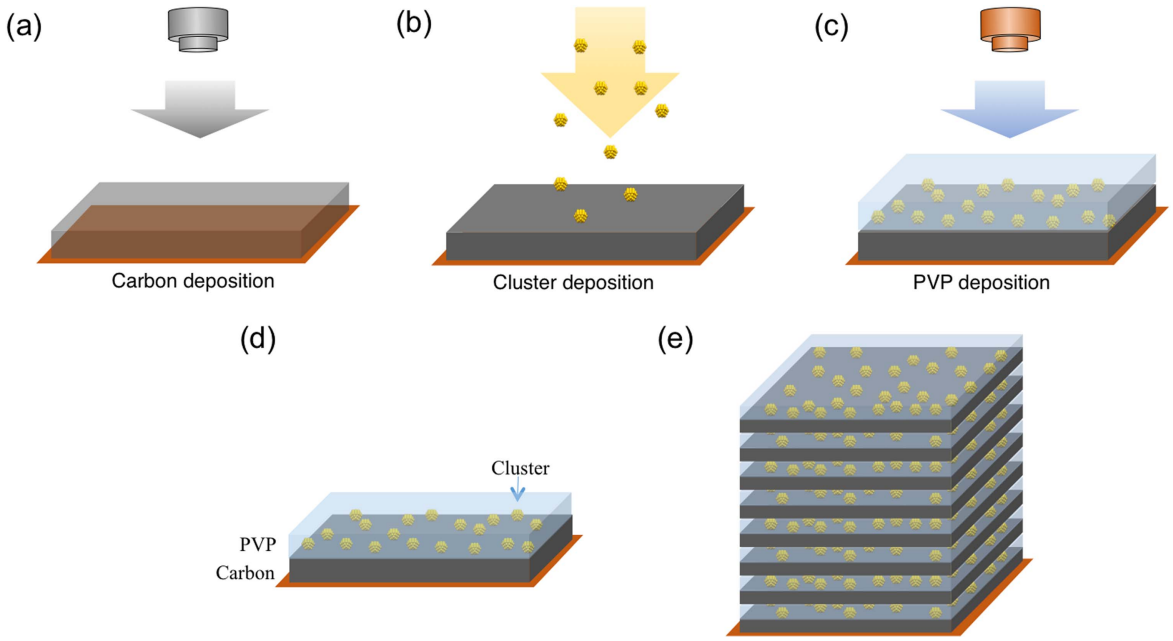

Figure 1. Schematic of the multilayer deposition process: (a) the carbon layer was deposited onto the substrate by e-beam evaporation, (b) the Au clusters were deposited on top of the carbon layer, (c) the polymer (PVP) layer was formed on top of the cluster layer by either pulse valve spray deposition or thermal evaporation. Then (d) a carbon–cluster–PVP sandwich was formed. This process was repeated to form (e) a multilayer stack of carbon–cluster–PVP sandwiches.

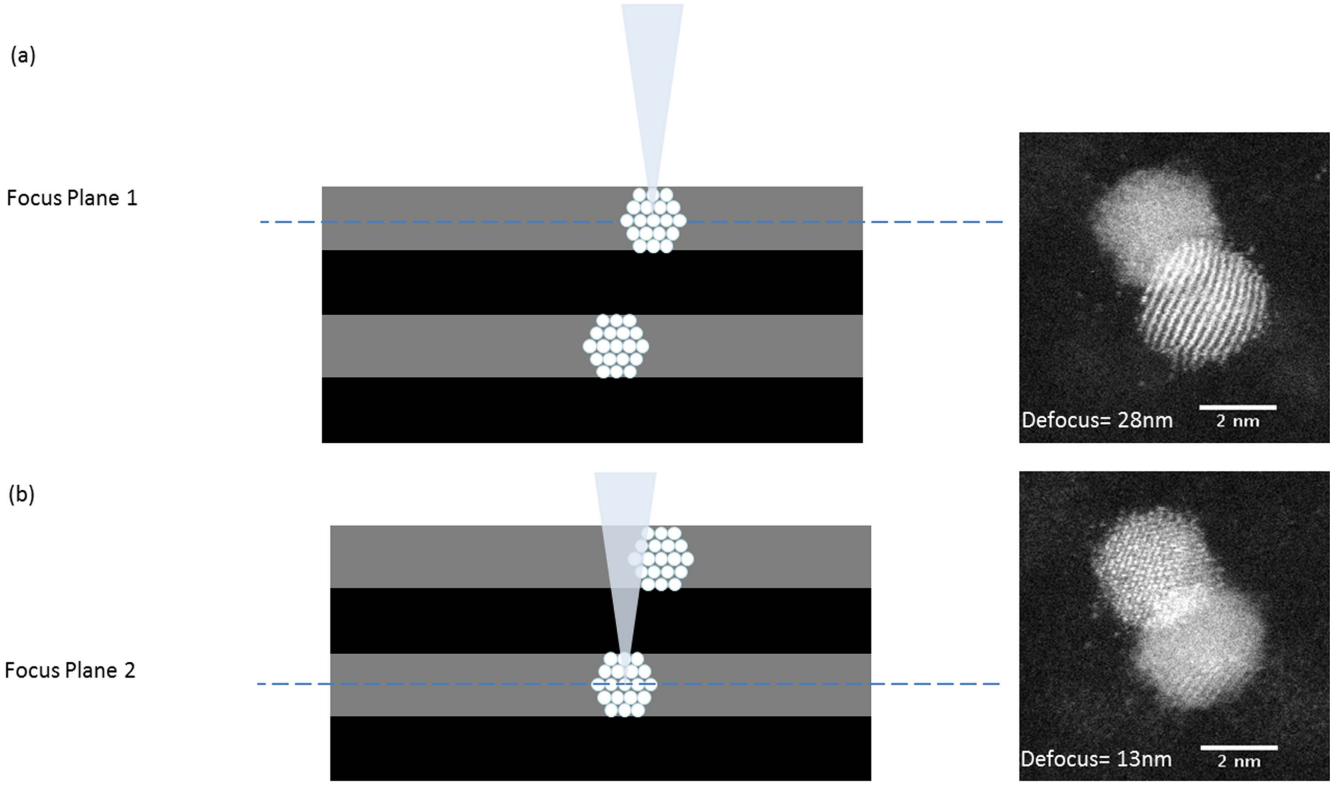

Figure 2. Schematic of the through-focal HAADF STEM analysis on the multilayer sample. The electron beam was focused on (a) the upper cluster and (b) the lower cluster. The cluster centres were estimated from their corresponding focal plane 1 and 2. Therefore, the defocus difference between these two planes corresponds to the thickness of one complete carbon–cluster–PVP sandwich.

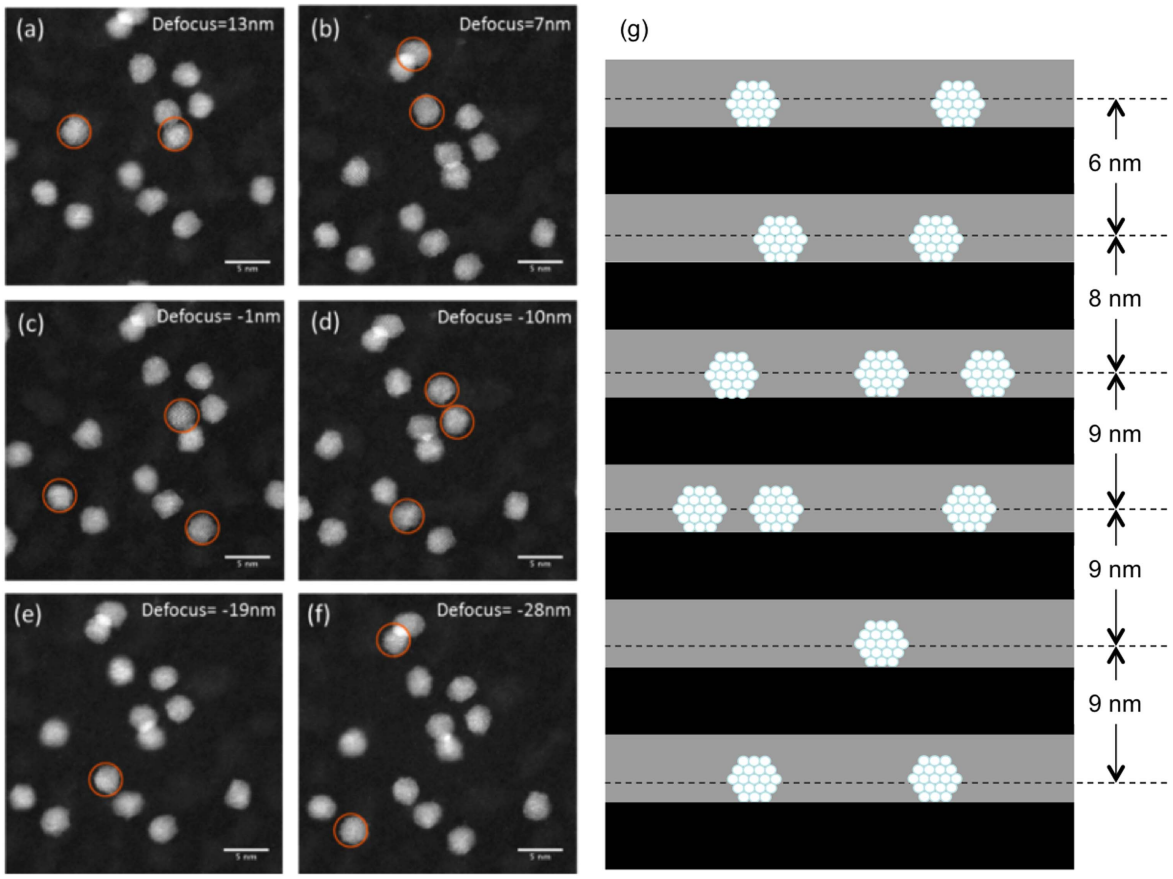

Figure 3. (a)–(f) Through-focal HAADF STEM images of a multilayer sample comprised of eight carbon–cluster–PVP sandwiches each deposited under the same conditions. The clusters in focus are marked by the red circles. (g) A schematic diagram of the 3D structure of the multilayer sample with the thickness values determined from the through-focal STEM analysis.

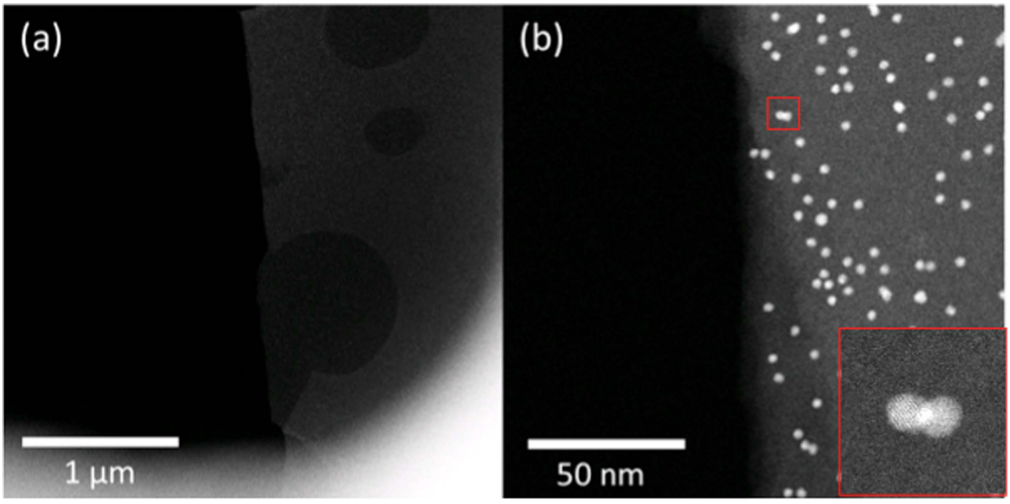

Figure 4. HAADF STEM images of the diced sample edge produced by diamond saw dicing with (a) low magnification and (b) medium magnification, showing the successful dicing with good edge morphology preservation of the multilayer structure after dicing. The inset in (b) shows two clusters whose profiles overlapped without coalescence, indicating that different layers are preserved even close to the dicing edge.

is even larger than the 41 nm difference in the 6-layer series. This suggests that there may be three more layers in this second series that have not been identified by the through-focal analysis due to the limited number of Au clusters happening to lie within any given lateral region for imaging.

The process of dicing of the multilayer films was carried out by an automatic mechanical dicer with a diamond saw. This method has been successfully employed previously to produce powder-supported size-selected clusters [35]. To check the effect of the dicing process on the multilayer sample, the multilayer

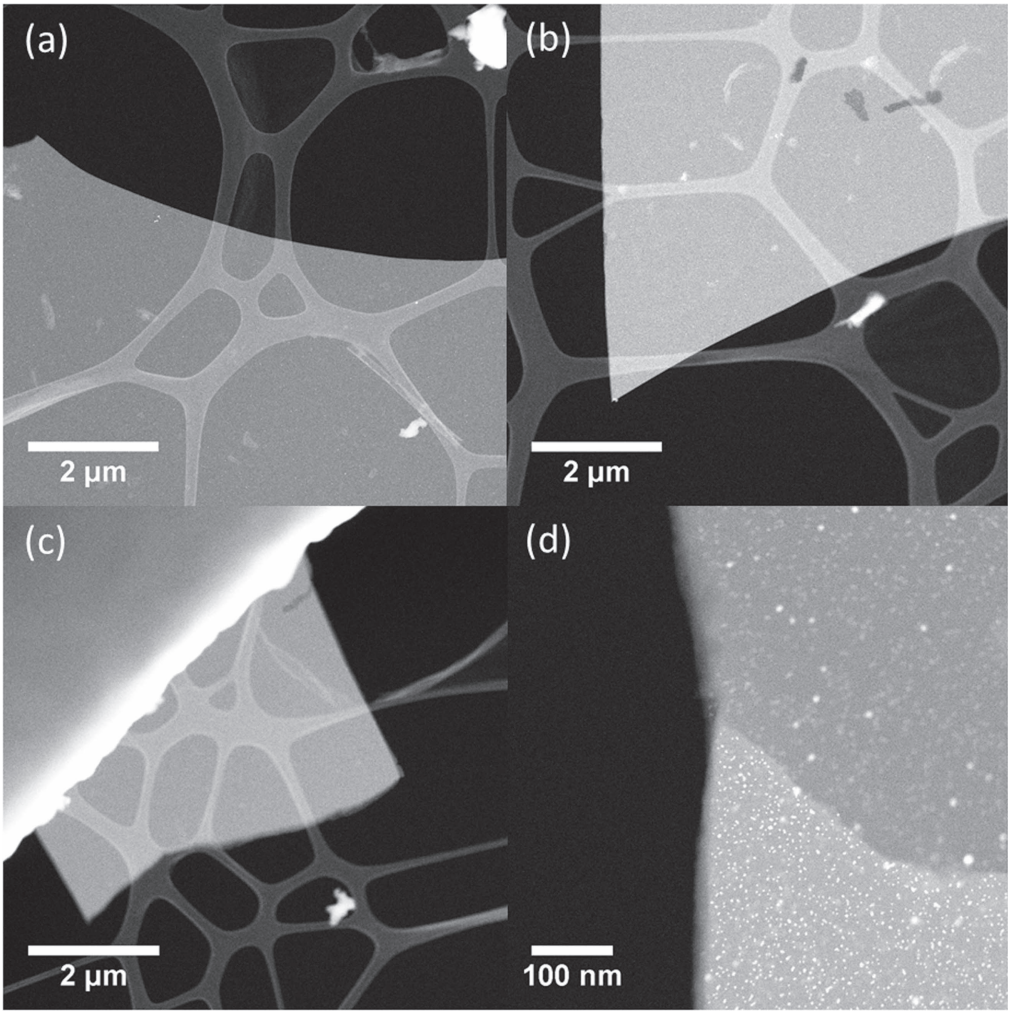

Figure 5. The HAADF STEM images of platelets with single, double and triple layers are shown in (a)–(c), respectively. A platelet with part single layer (upper) and part double layer (lower) is shown in (d).

sample deposited on the TEM grid was diced by a diamond saw into 0.5 mm × 0.5 mm pieces. Such pieces were then placed between two copper TEM grids without any additional support layer. The HAADF STEM images of the dicing edge are shown in figure 4, we can see that the dicing appears to leave good straight edges. The clusters were uniformly distributed across the sample even at the very edge of the diced pieces. Most significantly, it can be clearly seen in figure 4(b) that profiles of two (vertically separated) clusters overlap each other without aggregation, which indicates that the multilayer structure was still conserved after dicing (i.e. the clusters are in different layers).

In order to demonstrate the release process after dicing of the multilayers, samples comprised of a stack of ten carbon–cluster–PVP sandwiches were prepared on a silicon substrate using the method described above. These samples were diced and then placed in isopropanol for 2 h to dissolve the PVP layers and thus produce small carbon platelets bearing the Au clusters. After the platelets were released, they were deposited onto a TEM grid for imaging by HAADF STEM. The results are shown in figure 5, where it can be seen that the supported Au cluster platelets were successfully released from the multilayer samples. However, they do not appear to have been released as single layer platelets. Platelets comprising one, two and three layers can be seen in figures 5(a)–(c), respectively. The number of layers was obtained by characterization of clusters in different focal planes. It seems that some of the carbon layers remained bound in small stacks after the 'release' step. In figure 5(d), platelets with both single layer regions and double layer regions are observed. These results illustrate the principle that small Au cluster bearing carbon platelets can be released from the multilayer carbon–cluster–PVP stacks. The surviving double and triple sandwich platelets suggest that more vigorous dissolution of the polymer layers is needed to generate single layers of clusters on carbon. In this case it seems the PVP release layers were not completely dissolved, e.g., because the PVP release layers deposited by pulse valve spraying may not be completely homogeneous.

Does the multilayer deposition process affect the cluster significantly, so as to diminish the advantages of the cluster beam deposition? Does the deposition of carbon and PVP layers and the release process change cluster size distribution? The

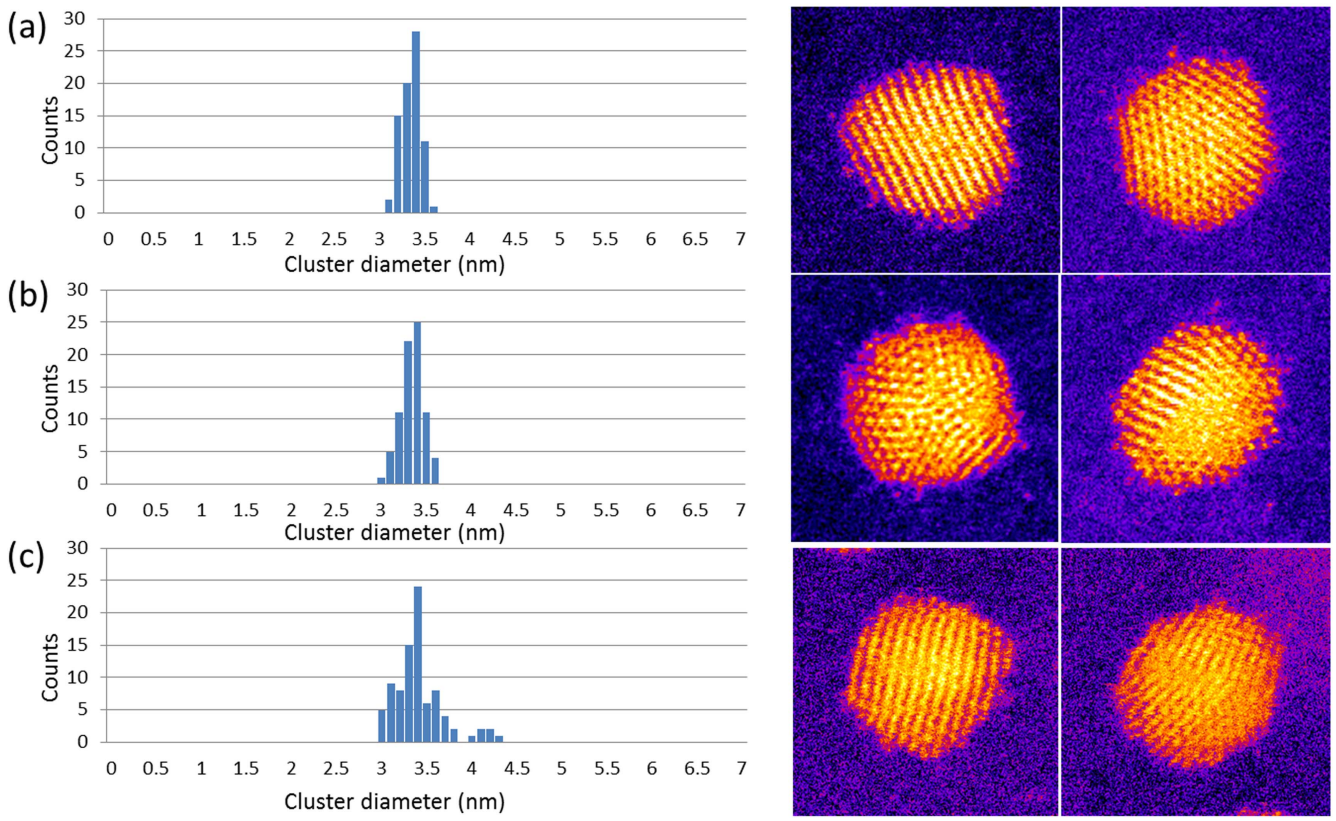

Figure 6. The diameter distribution and the corresponding representative HAADF STEM images of the clusters from (a) as-deposited size-selected Au_{923} clusters, (b) Au clusters in the multilayer sandwiches and (c) Au clusters after dicing and release. The frame size of the STEM images is 5.04 nm × 5.04 nm.

geometric sizes of Au clusters from an unreleased multilayer sample and a released multilayer sample are compared with Au clusters after normal cluster deposition with the same cluster source experimental conditions in figure 6. We see that the peak diameters are basically the same. The Au clusters in the multilayer sandwich stack show nearly the same distribution as the normal deposited clusters, suggesting that the carbon and PVP layers have little influence on the nanoclusters. In the released sample, the Au clusters have a somewhat wider size distribution, with the appearance of some aggregation, showing some influence of the release process on the clusters, probably due to some aggregation during the dissolution step. But the main peak of the size distribution is still reasonably narrow (3.4 ± 0.2 nm), and in many cases the effect of the release process will probably be acceptable.

4. Conclusions

In summary, a novel method for the collection of deposited clusters has been demonstrated, which should in future be scalable to high cluster beam fluxes simply be extending the lateral and vertical dimensions of the samples generated. The method is based on the creation of multilayer stacks of carbon–cluster–PVP sandwiches. The clusters survive the multilayer deposition with size and shape conserved. Through-focal aberration-corrected HAADF STEM measurements were employed to confirm the multilayer structure of the stacks and successfully measure the thickness of the carbon–cluster–PVP sandwiches. Dicing of the stacks can be accomplished without very significant effect on the clusters. Carbon platelets bearing supported Au clusters can be released from the multilayer stacks by dissolving the PVP layers in isopropanol. The multilayer deposition method that has been developed here has promise for applications including large-scale supported catalyst production with the next generation of high flux cluster beam sources such as MACS. The multilayer stacks produced can be regarded as a new architecture for storing supported catalyst particles, and may offer better interim protection for the clusters than direct deposition onto powder supports. Future work may address the morphology of the PVP layer in particular, with the aim of achieving closer to 100% release of single supported cluster layers after release, as well as automation of the whole multilayer deposition process, and especially the dicing step, to increase the process speed radically.

Acknowledgments

We thank Vitor Oiko from NPRL, University of Birmingham for his help with the carbon evaporator test. We acknowledge financial support from the EPSRC and TSB/Innovate UK. The STEM and cluster beam source instrument employed in this research were obtained through the Birmingham Science

City project 'Creating and Characterizing Next Generation Advanced Materials,' supported by Advantage West Midlands (AWM) and in part funded by the European Regional Development Fund (ERDF).

References

[1] Baletto F and Ferrando R 2005 Structural properties of nanoclusters: energetic, thermodynamic, and kinetic effects *Rev. Mod. Phys.* **77** 371–423

[2] Ferrando R, Jellinek J and Johnston R L 2008 Nanoalloys: from theory to applications of alloy clusters and nanoparticles *Chem. Rev.* **108** 845–910

[3] Schmid G, Baumle M, Geerkens M, Heim I, Osemann C and Sawitowski T 1999 Current and future applications of nanoclusters *Chem. Soc. Rev.* **28** 179–85

[4] Toshima N and Yonezawa T 1998 Bimetallic nanoparticles—novel materials for chemical and physical applications *New J. Chem.* **22** 1179–201

[5] Templeton A C, Wuelfing W P and Murray R W 2000 Monolayer-protected cluster molecules *Acc. Chem. Res.* **33** 27–36

[6] Judai K, Abbet S, Wörz A S, Heiz U and Henry C R 2004 Low-temperature cluster catalysis *J. Am. Chem. Soc.* **126** 2732–7

[7] Burch R 2006 Gold catalysts for pure hydrogen production in the water-gas shift reaction: activity, structure and reaction mechanism *Phys. Chem. Chem. Phys.* **8** 5483–500

[8] Klein D L, Roth R, Lim A K L, Alivisatos A P and McEuen P L 1997 A single-electron transistor made from a cadmium selenide nanocrystal *Nature* **389** 699–701

[9] Chi L, Hartig M, Drechsler T, Schwaack T, Seidel C, Fuchs H and Schmid G 1998 Single-electron tunneling in Au_{55} cluster monolayers *Appl. Phys.* A **190** 187–90

[10] Buchenau H, Knuth E L, Northby J, Toennies J P and Winkler C 1990 Mass spectra and time-of-flight distributions of helium cluster beams *J. Chem. Phys.* **92** 6875–89

[11] Pratontep S, Carroll S J, Xirouchaki C, Streun M and Palmer R E 2005 Size-selected cluster beam source based on radio frequency magnetron plasma sputtering and gas condensation *Rev. Sci. Instrum.* **76** 045103

[12] Duval P B, Burns C J, Clark D L, Morris D E, Scott B L, Thompson J D, Werkema E L, Jia L and Andersen R A 2001 Synthesis and structural characterization of the first uranium cluster containing an isopolyoxometalate core *Angew. Chem., Int. Ed. Engl.* **13** 3357–61

[13] Maity P, Xie S, Yamauchi M and Tsukuda T 2014 Stabilized gold clusters: from isolation toward controlled synthesis *Nanoscale* **4** 4027–37

[14] Ghosh A and Pradeep T 2014 Synthesis of atomically precise silver clusters by using the miscibility principle *Eur. J. Inorg. Chem.* **31** 5271–5

[15] Huard D J E, Kane K M and Tezcan F A 2013 Re-engineering protein interfaces yields copper-inducible ferritin cage assembly *Nat. Chem. Biol.* **9** 169–76

[16] Thakkar K N, Mhatre S S and Parikh R Y 2010 Biological synthesis of metallic nanoparticles *Nanomed. Nanotechnol., Biol. Med.* **6** 257–62

[17] Song J Y and Kim B S 2009 Rapid biological synthesis of silver nanoparticles using plant leaf extracts *Bioprocess Biosyst. Eng.* **32** 79–84

[18] Wegner K, Piseri P, Tafreshi H V and Milani P 2006 Cluster beam deposition: a tool for nanoscale science and technology *J. Phys. D: Appl. Phys.* **39** R439–59

[19] Palmer R E, Cao L and Yin F 2016 Note: proof of principle of a new type of cluster beam source with potential for scale-up *Rev. Sci. Instrum.* **87** 046103

[20] Ellis P, Brown C M, Bishop P T, Yin J, Cooke K, Terry W D, Liu J, Yin F and Palmer R E 2016 The cluster beam route to model catalysts and beyond *Faraday Discuss.* **188** 39–56

[21] Oiko V T A, Mathieu T, Cao L, Liu J and Palmer R E 2016 Note: production of silver nanoclusters using a matrix-assembly cluster source with a solid CO_2 matrix *J. Chem. Phys.* **145** 166101

[22] Merrifield R, Wang Z, Palmer R and Lead J 2013 Synthesis and characterization of polyvinylpyrrolidone coated cerium oxide nanoparticles *Environ. Sci. Technol.* **47** 12426–33

[23] Xiong Y, Washio I, Chen J, Cai H, Li Z Y and Xia Y 2006 Poly (vinyl pyrrolidone): a dual functional reductant and stabilizer for the facile synthesis of noble metal nanoplates in aqueous solutions *Langmuir* **22** 8563–70

[24] Xian J, Hua Q, Jiang Z, Ma Y and Huang W 2012 Size-dependent interaction of the poly (N-vinyl-2-pyrrolidone) capping ligand with Pd nanocrystals *Langmuir* **28** 6736–41

[25] Tsunoyama H, Ichikuni N and Tsukuda T 2008 Microfluidic synthesis and catalytic application of PVP-stabilized, ~1 nm gold clusters *Langmuir* **24** 11327–30

[26] Sun Y G and Xia Y N 2002 Shape-controlled synthesis of gold and silver nanoparticles *Science* **298** 2176–9

[27] Zhang Q, Lee J Y, Yang J, Boothroyd C and Zhang J 2007 Size and composition tunable Ag–Au alloy nanoparticles by replacement reactions *Nanotechnology* **18** 245605

[28] Turner M, Golovko V B, Vaughan O P H, Abdulkin P, Berenguer-Murcia A, Tikhov M S, Johnson B F G and Lambert R M 2008 Selective oxidation with dioxygen by gold nanoparticle catalysts derived from 55-atom clusters *Nature* **454** 981–3

[29] von Issendorff B and Palmer R E 1999 A new high transmission infinite range mass selector for cluster and nanoparticle beams *Rev. Sci. Instrum.* **70** 4497

[30] Pratontep S, Preece P, Xirouchaki C, Palmer R E, Sanz-Navarro C F, Kenny S D and Smith R 2003 Scaling relations for implantation of size-selected Au, Ag, and Si clusters into graphite *Phys. Rev. Lett.* **90** 055503

[31] Dahmen U, Erni R, Radmilovic V, Kisielowski C, Rossell M and Denes P 2009 Background, status and future of the transmission electron aberration-corrected microscope project *Phil. Trans. R. Soc.* A **367** 3795–808

[32] Pennycook S J, Lupini A R, Varela M, Borisevich A Y, Peng Y, Oxley M P and Chisholm M F 2006 Scanning transmission electron microscopy for nanostructure characterization *Scanning Microscopy for Nanotechnology: Techniques and Applications* ed W Zhou and Z L Wang (Berlin: Springer) pp 152–91

[33] Kisielowski C *et al* 2008 Detection of single atoms and buried defects in three dimensions by aberration-corrected electron microscope with 0.5 A information limit *Microsc. Microanal.* **14** 469–77

[34] van Benthem K, Lupini A R, Oxley M P, Indlay S D, llen L J and Pennycook S J 2006 Three-dimensional ADF imaging of individual atoms by through-focal series scanning transmission electron microscopy *Ultramicroscopy* **106** 1062–8

[35] Habibpour V, Song M Y, Wang Z W, Cookson J, Brown C M, Bishop P T and Palmer R E 2012 Novel powder-supported size-selected clusters for heterogeneous catalysis under realistic reaction conditions *J. Phys. Chem.* C **116** 26295–9